Journal of Materials Chemistry A

ROYAL SOCIETY OF CHEMISTRY

PAPER

View Article Online
View Journal | View Issue

Cite this: J. Mater. Chem. A, 2025, 13, 13205

Thermally-induced agglomeration tailors the stability of Pt SAs on TiO_2 and use in photocatalytic H_2 generation†

Johannes Will, *[a] Nikita Denisov,[b] Shanshan Qin, [b] Mingjian Wu, [a] Yue Wang,[b] Hyesung Kim,[b] Nicolas Karpstein, [a] Martin Dierner,[a] Patrik Schmuki *[bc] and Erdmann Spiecker [a]

Thermally-induced agglomeration of Pt single atoms (SAs) on anatase TiO_2 thin films is exploited for tuning their activity in photocatalytic H_2 generation. After thermal treatment at temperatures ranging from 350 to 650 °C in an Ar atmosphere, a more than fivefold higher photocatalytic activity is achieved under optimized conditions. The Pt species obtained after annealing at different temperatures are monitored *via ex situ* and *in situ* transmission electron microscopy. For *in situ* measurements, a gas cell system operating at 700 mbar is utilized. Structural data obtained in the temperature range from 250 to 950 °C demonstrate the co-existence of SA species and agglomerates over the whole temperature range, and give fundamental insights into thermal and light-induced agglomeration processes, including nucleation, growth and ripening of Pt species on TiO_2. Under optimized annealing conditions Pt is present as a mixture of SAs, 2D rafts and nanoparticles. Data show that annealing can stabilize the Pt species against light-induced agglomeration and detailed analysis reveals such SAs (realized under optimized annealing conditions) provide the most active sites (in comparison with various agglomerates). We further emphasize the importance of conducting atomic-scale structural characterization both before and after photocatalysis to accurately establish the process–structure–property–performance relationships of SAs in photocatalysis.

Received 31st January 2025
Accepted 24th March 2025

DOI: 10.1039/d5ta00843c

rsc.li/materials-a

Engineering of atomically dispersed metal sites has recently drawn tremendous research attention, with clearly foreseeable applications in the fields of catalysis, energy conversion and storage, and biomedicine. Particularly, in heterogeneous catalysis and photocatalysis, where supported active noble-metal clusters play a crucial role in the performance, the feasibility of downscaling their dimensions to the size of single atoms (SAs) offers remarkable benefits for the cost-efficiency and potentially the reactivity of the resulting catalysts.[1–5] Owing to maximized exposure of isolated atoms to the reaction medium/interface, SA active sites are far superior to traditional nanoparticles (NPs) in terms of atomic utilization efficiency.[6–9] At the same time, they offer some promising features, such as unique selectivity in catalyzing certain reactions,[10–12] as well as tunable electronic properties and activity depending on the coordination environment[13,14] and could thus prospectively further advance the solar-to-hydrogen efficiency in photocatalytic water splitting which recently already exceeded 9%.[15]

Despite the significant progress made in recent years, a major obstacle to the applicability of many SA-based catalytic systems remains their stability.[16] Due to their high surface energy as well as weak metal–support bonding, most supported noble metal SAs show a tendency to agglomerate under reaction conditions.[17–19] The consequences can be clearly detrimental not only due to the loss of active surface area, but also due to size-related effects on the adsorbate binding at the active sites – *i.e.*, the latter could potentially become inactive in the desired reactions (such as H_2 evolution). On the other hand, recent investigations on light-induced agglomeration of Pt on TiO_2 (ref. 17) reveal a stable activity although only ~6% of the Pt stays in its SA state.

The rationale behind this finding is not clear, but studies which aim at identifying the nature of top-performing Pt species reveal that not all Pt SAs contribute equally to the photocatalytic activity[20] and that under usual photocatalytic HER conditions, low Pt loading is good enough to achieve a maximized co-

[a]Institute of Micro- and Nanostructure Research & Center for Nanoanalysis and Electron Microscopy (CENEM), Friedrich-Alexander-Universität Erlangen-Nürnberg, IZNF, Cauerstraße 3, 91058 Erlangen, Germany. E-mail: johannes.will@fau.de
[b]Department of Materials Science WW4-LKO, Friedrich-Alexander-Universität Erlangen-Nürnberg, Martensstrasse 7, 91058 Erlangen, Germany. E-mail: schmuki@ww.uni-erlangen.de
[c]Regional Centre of Advanced Technologies and Materials, Czech Advanced Technology and Research Institute, Palacky University, Olomouc, 779 00, Czech Republic

† Electronic supplementary information (ESI) available: Experimental methods including TiO_2 layer and subsequent Pt SA deposition, STEM imaging conditions, temperature profiles, complementary STEM images, post-mortem characterization and *in situ* SAED patterns of TiO_2 crystallization. See DOI: https://doi.org/10.1039/d5ta00843c

catalytic effect.[21] This can have several reasons, *e.g.*, the varying intrinsic activity of different SAs due to the varying Pt–support interaction or a higher activity of agglomerated Pt species as compared to their SA state. In the literature various species such as ~1 nm Pt clusters,[22–25] 0.2 nm PtO species,[26] rafts below a size of ~10 atoms[21] and dual atom sites[27–29] have been identified to contribute primarily to the total activity. Additionally, the co-existence of SAs with rafts and intrinsic defects can have beneficial effects.[30–33] In contrast, larger Pt agglomerates, predominantly consisting of Pt^0 species (metallic nanoparticles), seem to not substantially contribute to the overall photocatalytic activity.[20,21,23] Thus, studying gentle thermally-induced SA agglomeration might be an expedient strategy to extract beneficial and detrimental Pt configurations for photocatalytic applications.

Surprisingly, studies on thermally-induced agglomeration of SAs on TiO_2 and the connection of agglomerates with activity are scarce.[5,24] Regarding thermal agglomeration, it has been established that the agglomeration depends on both the annealing atmosphere and the metal–support interaction.[16,23] The observed effects indicate phenomena including agglomeration into amorphous clusters or crystalline nanoparticles,[23,34–37] NP redispersion into SAs,[35,38–42] or encapsulation of Pt species into a TiO_x shell.[23,37,43,44] For thermally-induced agglomeration of Pt to nanoparticles on SiO_2 as well as Al_2O_3 it was found that a particle size dependent activation energy for Pt detachment[45] and Pt attachment[46] is needed to describe the observed agglomeration behavior during Ostwald ripening.[47,48] Notably, Ostwald ripening as an acting mechanism and some studies on ceria-based SA catalysts[49] underscore the importance of a competition between agglomeration and dispersion of Pt species. Accordingly, for Pt on TiO_2 for thermally-induced agglomeration of Pt, co-existence of agglomerated and dispersed Pt species may be expected – however, a systematic study with atomic resolution is missing.

Therefore, in this study, we systematically investigate the influence of inert Ar annealing conditions over a wide temperature range on the Pt atomic surface configurations as well as the resulting photocatalytic activity of Pt on TiO_2 thin films. The Pt on the TiO_2 thin film model system enables comprehensive structural and chemical characterization *via* high-resolution scanning transmission electron microscopy (HR-STEM) and correlative X-ray photoelectron spectroscopy (XPS), both revealing the co-existence of dispersed and agglomerated Pt species with different ratios and varying cluster sizes at different temperatures. For a better understanding of the acting agglomeration mechanism, *in situ* electron microscopy in a gas cell (DENSsolution climate chip) was conducted in an Ar atmosphere (700 mbar) up to 950 °C. The *in situ* data elucidates the first steps of agglomeration, including non-classical nucleation of Pt SAs, the detachment of Pt from already existing NPs and the changing temperature-dependent balance between dispersed SA and agglomerated Pt species with a high degree of redispersion at elevated temperatures. Finally, we investigate the Pt configuration of the pre-annealed and as-deposited samples after photocatalysis, shedding light on the impact of the thermally pre-agglomerated state on its stability under illumination. The correlation of the structural characterization with the photocatalytic activity suggests that SAs, which are preserved after both thermal annealing and photocatalysis, represent super-performing catalytic sites that provide the main catalytic activity.

Effect of temperature on photocatalytic H_2 activity of Pt SA decorated TiO_2

To study the impact of thermal Ar annealing on the photocatalytic activity of Pt loaded TiO_2 samples, first 20 nm thick TiO_2 films were sputtered on Si/SiO_2 (*cf.* Fig. S1†) and annealed at 450 °C to crystallize the thin films as described above. The crystallized anatase films where then immersed in a 2 mM H_2PtCl_6 solution for 24 h leading to highly dispersed Pt SAs on the surface.[41,50] The films were then annealed in an Ar atmosphere in a temperature range from 350 to 650 °C. Subsequently the photocatalytic activity was determined in a quartz glass reactor under LED illumination at 275 nm at a power of 30 mW. Here, charge carriers (e^-/h^+ pairs), which further migrate to the surface and react with the surrounding aqueous environment, are generated in the anatase thin films. The resulting hydrogen evolution data, which is displayed in Fig. 1 as well as in Fig. S2,† reveals a clear impact of the annealing conditions on the activity. Surprisingly, the activity is higher than that of the untreated sample independent of Ar temperature. Note that the Raman spectra (*c.f.* Fig. S3†) of the thin films after annealing at different temperatures reveal no changes in the TiO_2 anatase fingerprint nor the co-existence of other TiO_2 phases such as rutile, brookite, or TiO_2(B). In this context, other phases would influence the thermal and light-induced agglomeration behavior due to different bonding strengths due to their inherently different surface energetics.[51] Notably, the activity increases with increasing annealing temperature and peaks at 550 °C with an activity which is ~5.7 fold higher than that of the non-treated sample. In the following, we will elucidate the

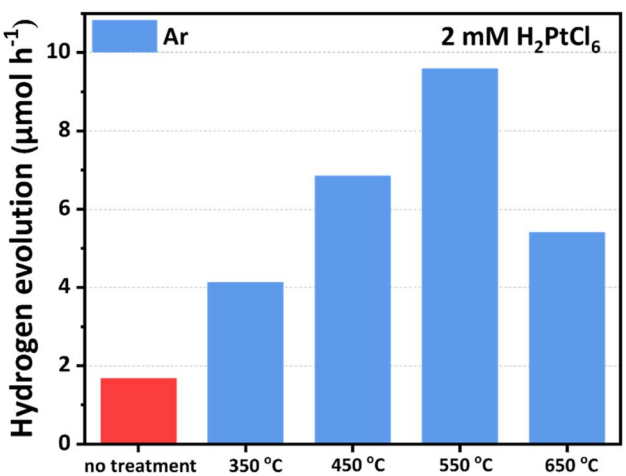

Fig. 1 Impact of thermal annealing in an Ar atmosphere on the photocatalytic activity of Pt dispersed on flat TiO_2 films.

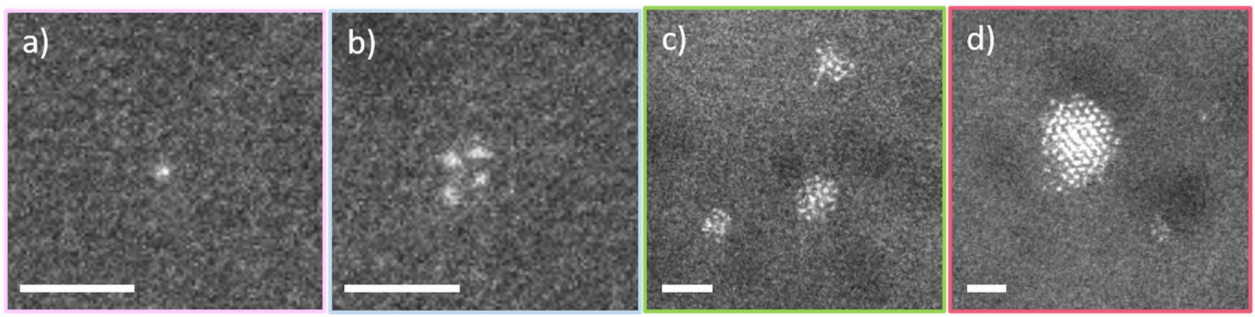

Fig. 2 Different types of Pt species typically co-existing on the TiO_2 support: (a) SA, (b) a few-atom raft, (c) rafts exhibiting a disordered structure, and (d) a NP showing lattice fringes (the scale bar corresponds to 1 nm).

corresponding Pt deposit morphology changes by the annealing and photocatalytic process by *ex situ* and *in situ* STEM investigations.

Impact of temperature on the thermal agglomeration behavior of Pt SAs on TiO_2

For high-angle annular dark-field (HAADF) imaging, 20 nm thick TiO_2 films were deposited and treated in the same way as the thin films for the activity measurements reported above. In the following we will discriminate between SAs, few-atom as well as larger amorphous rafts and crystalline Pt nanoparticles. Typical candidates of those species are exemplarily shown in Fig. 2, here the Z dependent contrast[52] in HAADF scanning transmission electron microscopy (STEM) imaging yields a good contrast even for Pt SAs supported on 20 nm TiO_2, which consequently appear bright in the micrographs. To prove the correlation of Pt with the bright spots in HAADF imaging, energy dispersive X-ray spectroscopy (EDXS) mapping of a typical TiO_2 surface was conducted (*c.f.* Fig. S4†) revealing a clear correlation between the Pt signal and HAADF NPs. The evolution in the Pt configuration after annealing is captured in Fig. 3. Similarly to Farnesi *et al.*[49] for Pt on ceria-based catalysts, a mixture of SAs and assemblies can be found independent of the annealing temperature. Additionally, a larger

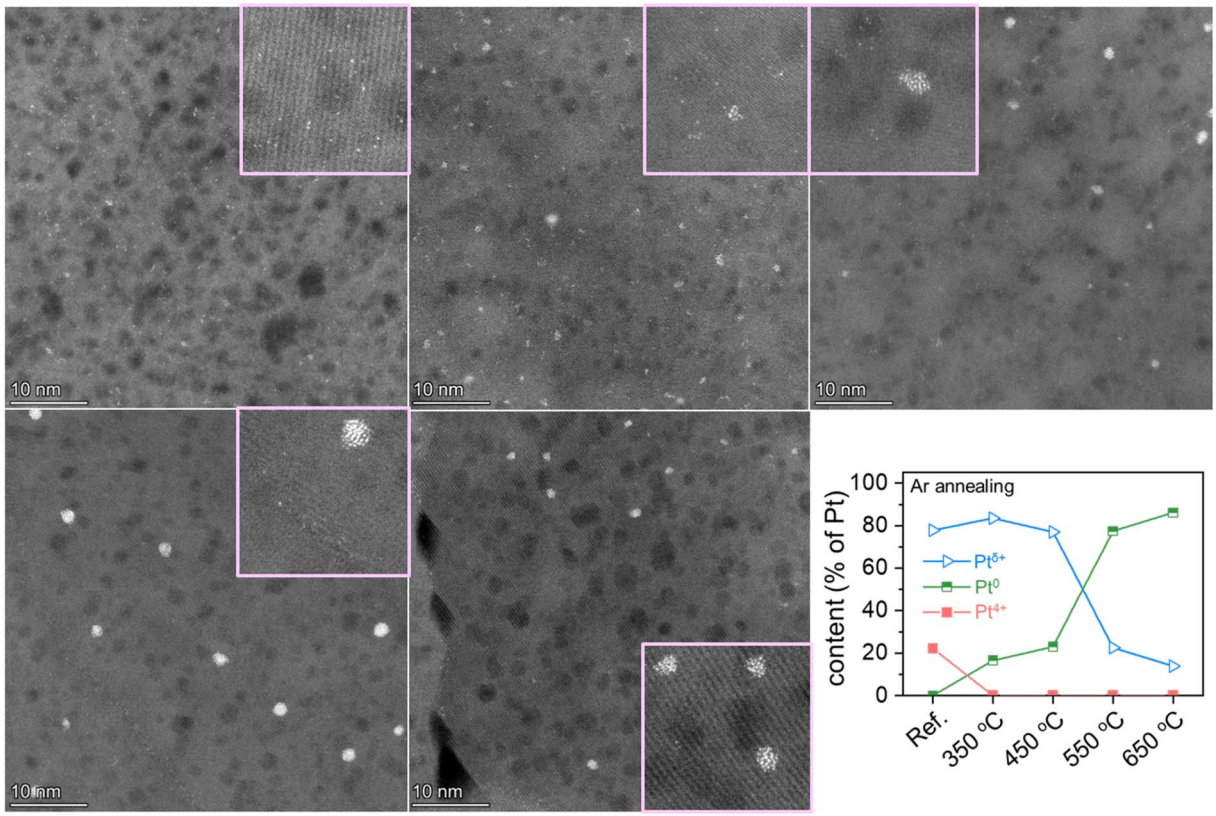

Fig. 3 Impact of thermal annealing in an argon atmosphere on the Pt dispersion and agglomeration on flat TiO_2 films (top left to bottom right: as-deposited; 350 °C, 1 h; 450 °C, 1 h; 550 °C, 1 h; 650 °C, 1 h; $Pt^{\delta+}$ to Pt^0 ratio as determined by XPS).

Table 1 Percentage of $Pt^{\delta+}$, density of SAs, rafts and NPs as well as the average NP size after different pre-annealing procedures

	As-deposited	350 °C, 1 h	450 °C, 1 h	550 °C, 1 h	650 °C, 1h
$Pt^{\delta+}$% (XPS)	77.8	83.5	77	22.6	13.9
#SA/μm^2	9×10^4	1×10^5	8×10^4	6×10^4	3×10^4
#Rafts/μm^2	1×10^4	5×10^3	1×10^4	2×10^4	3×10^3
#NPs/μm^2	0	1×10^4	1×10^3	1×10^4	3×10^3
d(NPs)/nm	n/A	1.6	1.7	2.3	1.8

degree of Pt agglomeration is visible with increasing temperature. Remarkably and similar to light-induced[17] or current-induced[18] agglomeration, Pt SAs always co-exist with their agglomerates even after annealing at 650 °C for 1 h. The co-existence of at least two species is also reflected *via* XPS (*cf.* Fig. 3, S5† and Table 1). Here, the XPS Pt $4f_{7/2}$ peak shifts gradually from ~72.6 eV to lower binding energies around ~71 eV. In accordance with the literature,[53] we assign one species to individual atom species $Pt^{\delta+}$ at 72.6 eV and another species to metallic Pt^0. The position of the Pt^0 peak deviates from that of a metal foil (~70.6 eV), and this deviation depends on the size of the Pt nanoparticles. This is because a larger fraction of Pt atoms at the surface experience a different electronic environment.[17] Additionally, the strong metal–support interaction (SMSI) between small Pt NPs and the TiO_2 support under thermal treatment in an O_2-free atmosphere may contribute to the shift of Pt 4f peaks from their standard positions, as reported in the literature.[54,55] Consequently, the position of the Pt^0 peak was used as a fitting parameter centered around ~71 eV. The resulting analysis of the XPS spectra yields a co-existence of $Pt^{\delta+}$ and Pt^0 species with a decreasing $Pt^{\delta+}$ fraction upon annealing. In order to quantify the degree of agglomeration with respect to the Pt species present, several STEM images for each sample were segmented by the Trainable Weka Segementation plugin of ImageJ (*c.f.* Methods section). The resulting density and size of Pt species are summarized in Table 1 revealing a decrease of the SA density in line with XPS analysis.

In general, the SA density decreases with increasing annealing temperature, still leaving 3×10^4 SAs per μm^2 on the TiO_2 support even after annealing at 650 °C. In addition, rafts as well as NPs with an average size of around 2 nm can be found on the support after thermal annealing. Note that a correlation of the as-deposited and annealed Pt configurations would at this stage suggest, for instance, that the SAs are not the active species and hint more at the NPs. This conclusion is, however, invalid since the Pt configuration upon illumination will change within minutes,[17] and thus the correlation of Pt surface-configuration and activity can only be made by investigating the Pt species after photocatalysis (*vide infra*).

Monitoring SAs and their thermal agglomeration behavior *in situ*

To shed further light on the thermal agglomeration process of Pt on TiO_2 on the atomic scale, *in situ* HAADF-STEM studies were performed aided by a gas cell setup schematically shown in Fig. S6.† Here, 20 nm thick amorphous TiO_2 layers were sputtered on the supporting TEM membranes (40 nm thick SiN_x) embedded within temperature-controlled silicon microchips (DENSsolutions). Next, an Ar atmosphere (700 mbar) was established within the sealed space above the TiO_2 surface, while the well-controlled heating[56] of the TiO_2-covered areas was directly provided by the heating elements within the microchips. Heating to 400 °C in this setup leads to crystallization of TiO_2 layers in the anatase phase, as confirmed by *in situ* selected area electron diffraction analysis (SAED, Fig. S7†).

The aforementioned setup was then utilized in the thermal studies of Pt SAs dispersed on the TiO_2 support (Fig. 4). Notably, upon introduction of an Ar atmosphere and heating, HAADF-STEM imaging of the Pt SAs becomes significantly more challenging. Most evidently, this is due to electron beam scattering effects within the cell, which includes ~70 nm thick SiN_x membranes and the ~1 μm thick Ar gas layer. Additionally, mobile SA species under elevated temperatures could be difficult to detect due to relatively slow image acquisition time (10 μs per pixel). Nevertheless, the structural evolution of immobilized Pt species (*e.g.* small nanoparticles, clusters or SAs immobilized on the support) under elevated temperatures can be reliably monitored *in situ*, owing to the significant difference in atomic number between Pt (78) and Ti (22).

Fig. 4 shows identical-location HAADF-STEM overview images of a Pt SA loaded (0.05 mM solution, reactive deposition[41]) TiO_2 layer heated in Ar in the temperature range from 250 °C to 950 °C (corresponding temperature profiles are provided in Fig. S8†). This location was specifically selected to show the influence of TiO_2 edges and grain boundaries (GB) in the polycrystalline TiO_2 structure on the thermally-induced processes. The images clearly reveal a strong Pt agglomeration tendency along the 2D defects, which can be subdivided into three stages: (1) nucleation of Pt agglomerates already at 250–350 °C; (2) further growth and sintering of the nuclei at 350–550 °C; (3) reduction in the NP density at 650–950 °C. This trend was further confirmed in additional series of HAADF-STEM studies obtained under the same conditions, but other magnifications or locations on the TEM grid (Fig. S9 and S10†).

Observed phenomena of thermally-induced SA agglomeration

The Pt agglomeration observed *in situ* is in line with the *ex situ* characterization of the 2 mM samples described above. The *in situ* data adds valuable information on the history of the existing NPs and reveals that initially formed agglomerates can dissolve, whereas others act as starting points for further NP growth. In this context, Pt agglomeration is well-documented in

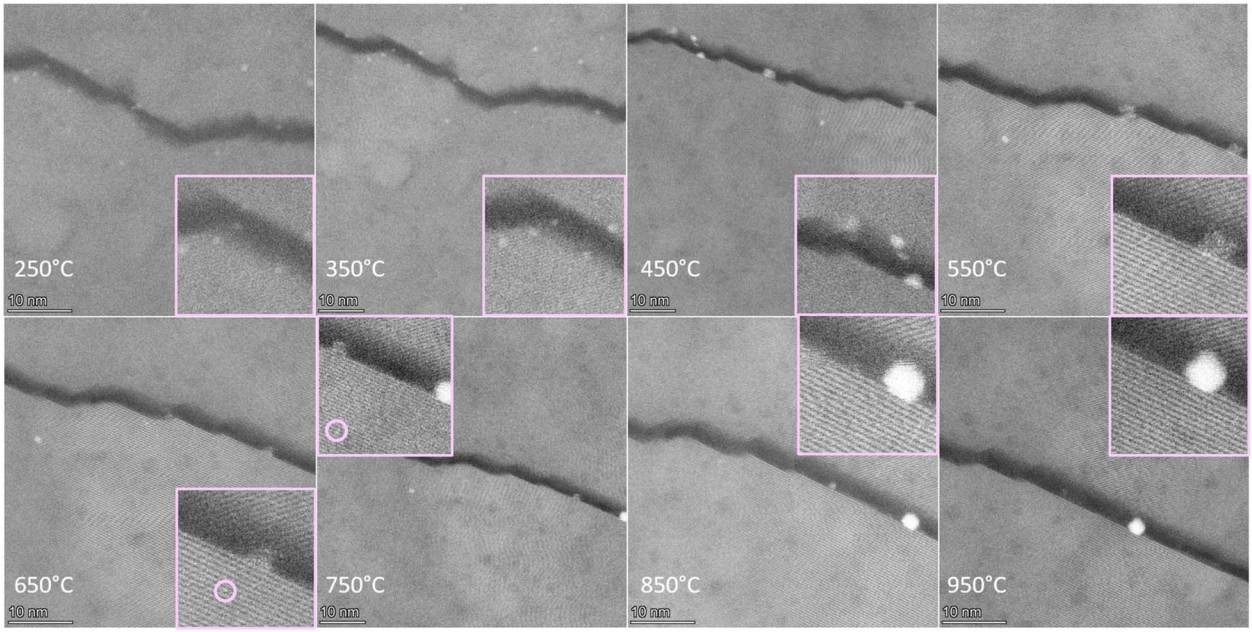

Fig. 4 Identical-location *in situ* HAADF-STEM images of the Pt SA decorated TiO2 layer (using 0.05 mM H_2PtC_{l6}) heated in an Ar atmosphere (700 mbar) to different temperatures (250–950 °C). Pt species can be identified as bright spots on the TiO_2 surface (based on the significant difference in atomic number between Pt (78) and Ti (22), and the related scattering strength in HAADF-STEM imaging).

reductive atmospheres[23,49,57] where gas adsorption weakens the metal–support interaction facilitating Pt SA destabilization and mobilization.[23,57,58] In our case, utilizing an inert Ar atmosphere was crucial to prevent any external influence on the Pt–TiO_2 binding strength – thus the observed thermal destabilization of Pt SAs already at 250 °C confirms the intrinsically low diffusion barriers for Pt SAs on TiO_2.[59] It is also clear that the structural quality of the support plays a role in thermally-induced processes, based on preferential formation of NPs along the 2D defect. The latter can be ascribed to the defect-induced changes in the metal–support interaction, which either facilitate heterogeneous nucleation (*e.g. via* lowering the critical radius for nucleation[60]) or provide higher mobility of SAs along extended defects[61] (thus higher flux of Pt SAs towards the nuclei). The observed dynamics of NP coarsening at higher temperatures is in line with the Ostwald ripening mechanism of metastable Pt clusters and NPs, which reduces their total surface energy.[45–49,59]. Notably, this process implies the co-existence of Pt SAs and NPs on the surface, and assumes a size-dependent activation energy for atom detachment.[46] Accordingly, in our experiments the existence of non-aggregated Pt SAs at different temperatures (650–950 °C) could be resolved in individual images presented in Fig. 5 in line with the *ex situ* data of the 2 mM samples presented above.

The apparent decline in NP density at 650–950 °C with simultaneous observations of Pt SAs strongly suggests the possibility of thermally-induced NP redispersion into SAs. Accordingly, upon cooling down the supports from 950 °C to

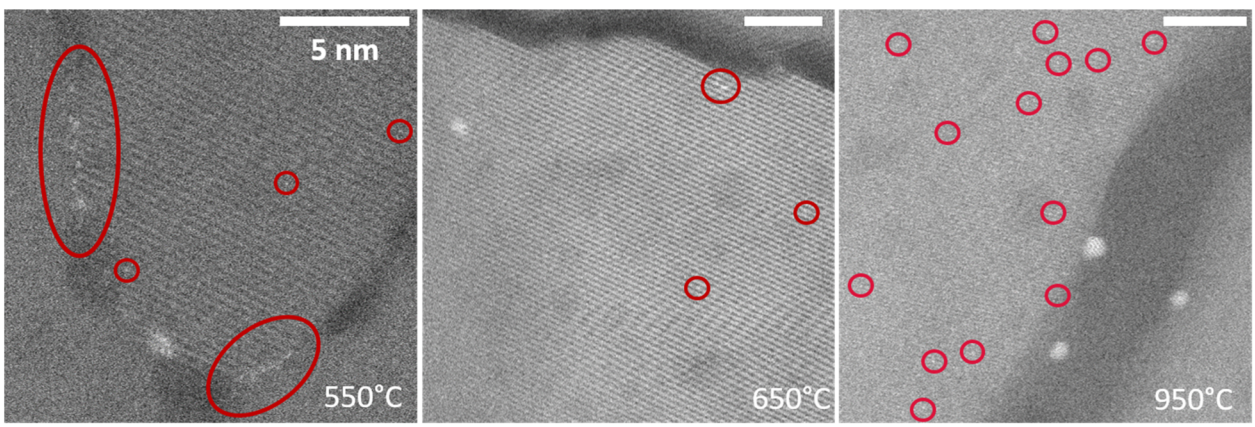

Fig. 5 High-magnification *in situ* HAADF-STEM observations of Pt SAs (highlighted) at different temperatures (following the same procedure as in Fig. 4). The scale bar in all images corresponds to 5 nm.

room temperature, we found abundant Pt SAs on the surface (Fig. S11†) and the preserved configuration of Pt agglomerates (Fig. S12†). This finding agrees with a previous report of the redispersion of Pt NPs under inert conditions and elevated temperatures.[62] To check if the observed redispersion into SAs also results in a high photocatalytic activity, a sample was annealed at 950 °C in an Ar atmosphere. The hydrogen evolution rate (Fig. S13†) is, however, lower as compared to all other samples. This effect might stem from a strong interaction of Pt with TiO_2 potentially leading to a TiO_2 overgrowth of Pt or Pt diffusion into the thin film and could be further investigated in the future.

Interplay of SAs and a NP: SA detachment and attachment monitored *in situ*

To gain further insights into the thermally-induced transformations and redispersion of Pt NPs supported on TiO_2, we

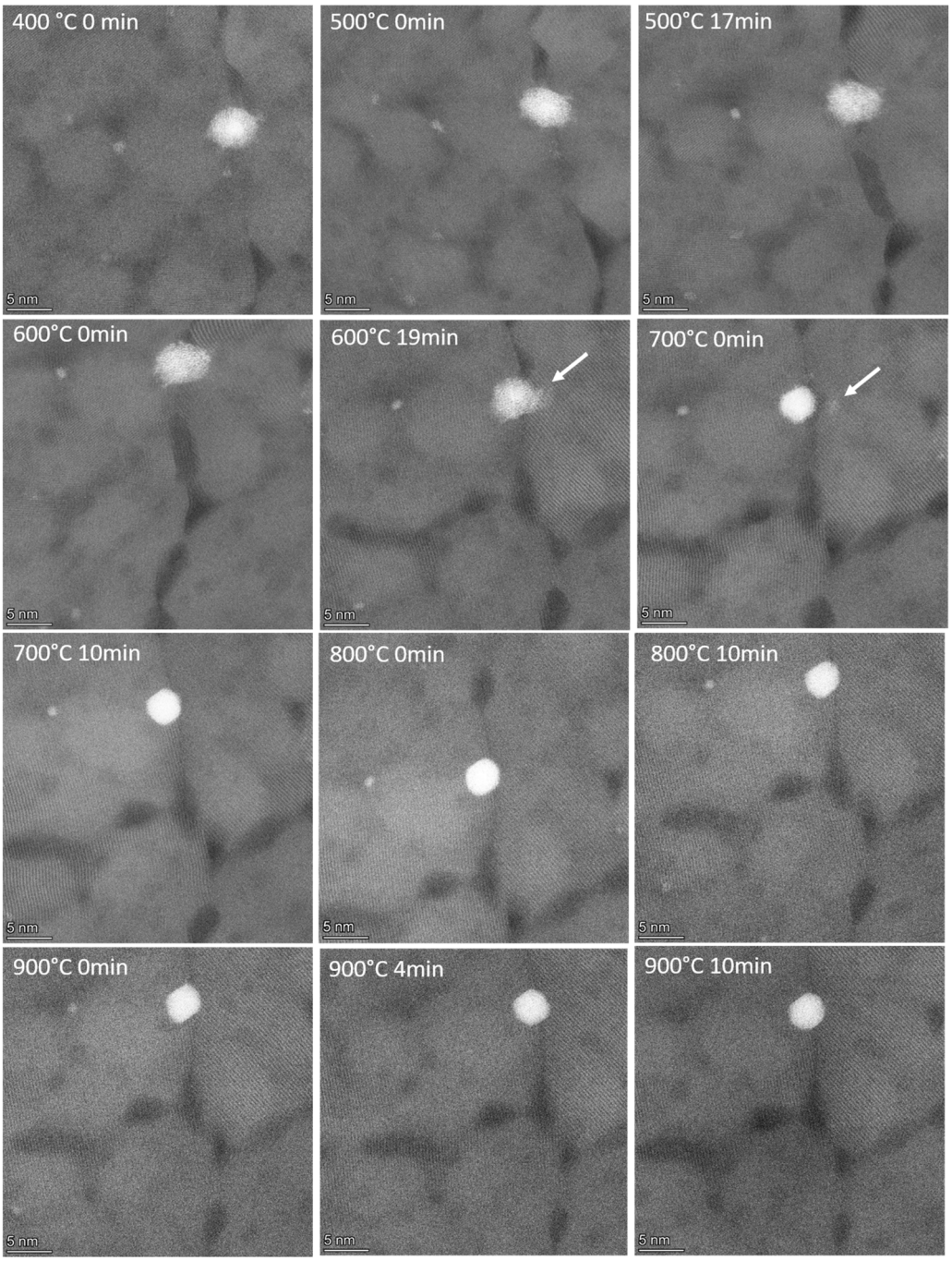

Fig. 6 High-magnification identical-location *in situ* HAADF-STEM imaging series showing the evolution of a Pt nucleus and its surroundings at 400–900 °C. The white arrow indicates the detachment of a Pt cluster from a larger particle.

carried out *in situ* identical-location observations of a Pt NP (~5 nm in diameter) at elevated temperatures, as presented in Fig. 6. Clearly, in the temperature range of 400–600 °C the NP appears as a metastable aggregate with ill-defined and overall unstable shape. Consequently, at the intermediate stage of heating (600 °C, 19 min–700 °C, 0 min) the metastable Pt agglomerate cleaves off a small cluster (marked by a white arrow). The detached Pt cloud appears to be spatially separated from the original NP by the grain boundary, and further disappears upon exposure to higher temperatures (700 °C, 10 min). This again suggests the competition between SA aggregation and redispersion in the Pt SA-TiO_2 system, although the latter process is activated at significantly higher temperatures. While such competition is implied in the Ostwald ripening mechanism, here it is experimentally verified by identical-location *in situ* HAADF-STEM with atomic resolution. The fact that smaller clusters are more prone to fragmentation/redispersion as compared to the larger agglomerates[63] agrees with a size-dependent activation energy for detachment (proportional to R^{-1} (ref. 45 and 46)) as a result of size-dependent surface energy.

With an increase in temperature from 600 °C to 700 °C (Fig. 6), a partially amorphous round-shaped and more flat Pt aggregate[30] (as revealed by STEM imaging) transforms into a compact, three-dimensional crystalline NP with distinct facets. Such reshaping and faceting of the investigated NP driven by the reduction of the surface energy is a common phenomenon for supported metal particles on oxide substrates,[64] and the size-dependent transition from a metastable liquid-like structure (at 400–600 °C) to the crystalline-ordered state (at 700–900 °C) is also in line with observations in colloidal systems at room temperature.[65]

Overall, the combined *ex situ* and *in situ* data reveal that the Pt configuration can be systematically tuned by thermal annealing. Pt tends to agglomerate *via* non-classical[60] heterogeneous nucleation and further agglomerates towards NPs. In addition, Ostwald ripening, the detachment of Pt species from existing agglomerates and the co-existence of SAs with NPs is observed over the whole temperature range. Thus, we can identify three major mechanisms: (i) attachment of Pt towards agglomerates, (ii) detachment of Pt from agglomerates, and (iii) SA diffusion on the TiO_2 support. While the attachment process is rather fast, the co-existence of SAs and agglomerates suggests that the detachment rate is on a similar timescale as compared to the residence time of SAs on the support. Here, the detachment rate, which is a temperature- as well as size- and morphology-dependent quantity, and the residence time are decisively influenced by the Pt binding energy to the agglomerate and the support, respectively. Thus, tuning the metal–support interaction[66] by changing the charge state of Pt[57,67,68] or the coordination environment by, *e.g.*, generating defects at the support Pt interface[30,53,69] can shift the SA-agglomerate balance towards the SA side. Alternatively, increasing the detachment rate by changing the surface or interface energies of Pt agglomerates by, *e.g.*, the annealing atmosphere[49,57] will lead to a similar effect. Another way to increase the mean free path for diffusion and thus the residence time on the support is tuning the Pt concentration: Here, very dilute SA configurations are found to be stable against sintering as well described in the literature.[16,70] In line with these findings, we observed almost no Pt thermal aggregation at lower SA loading (produced using 0.005 mM precursor solution) on the TiO_2 surface (Fig. S14†).

Pre-annealing as a remedy against light-induced agglomeration and identification of active sites

While thermal agglomeration is activated by temperature, light-induced and current-induced agglomeration are activated by a weakening of the metal–substrate interaction due to H adsorption.[17,18] Thus, it is interesting to see how light-induced agglomeration interacts with thermally pre-agglomerated species. For that, the as-deposited as well as the annealed samples were investigated after photocatalysis under illumination at 275 nm (30 mW) for 3 h. The resulting Pt configurations are exemplarily shown in Fig. 7 and summarized after segmentation (*vide supra*) in Table 2. Interestingly the SA density after photocatalysis is the lowest for the least active sample; thus, light-induced agglomeration acted the most on the non-annealed/as-deposited sample. One likely reason can be the generation of oxygen vacancies (O_Vs) during thermal annealing in an Ar atmosphere, which has been found for powder samples by electron paramagnetic resonance (EPR) in the past.[71] Here, EPR reveals a maximum density of O_Vs after annealing at 500 °C, those vacancies are then potential sites stabilizing SAs during photocatalysis. As can be seen by, *e.g.*, the average NP size or the final SA density, all samples underwent further agglomeration, while the raft density is reduced (except for 650 °C). In contrast to the solely thermally agglomerated state, the most active samples (450 and 550 °C) exhibit the lowest NP density, thus NPs can be excluded as main active sites. Similarly, the raft density is the highest for 650 °C and quite low for 450 °C, also indicating that rafts alone are not the most efficient activity contributors. All annealed samples, however, exhibit a higher SA density as compared to the as-deposited sample indicating that SAs are responsible for the activity. We also note that the 650 °C sample, although being in a similar range to the other most active samples, exhibits the highest SA density, which is a strong indication that not all SAs exhibit the same activity, in line with previous findings.[20,21] Interestingly, the correlation with XPS data (*cf.* Fig. 7 and Table 2) reveals that the most active samples exhibit the highest abundance of $Pt^{\delta+}$ species. However, the amount of $Pt^{\delta+}$ detected by XPS follows the activity trend, but decreases significantly compared to the density of SAs observed by STEM (*cf.* Table 1 and Fig. S15†). While a fairly linear relationship between SA density and $Pt^{\delta+}$ species exists after annealing, this relationship breaks down following photocatalysis. This suggests that not all structural SAs (STEM) are in the same electronic state (XPS), highlighting the importance of stabilizing SAs at the appropriate substrate sites to maximize the efficiency of the co-catalyst.[5] In this context, recent studies revealed a massive impact of the exposed TiO_2 surface on the Pt SA coordination and

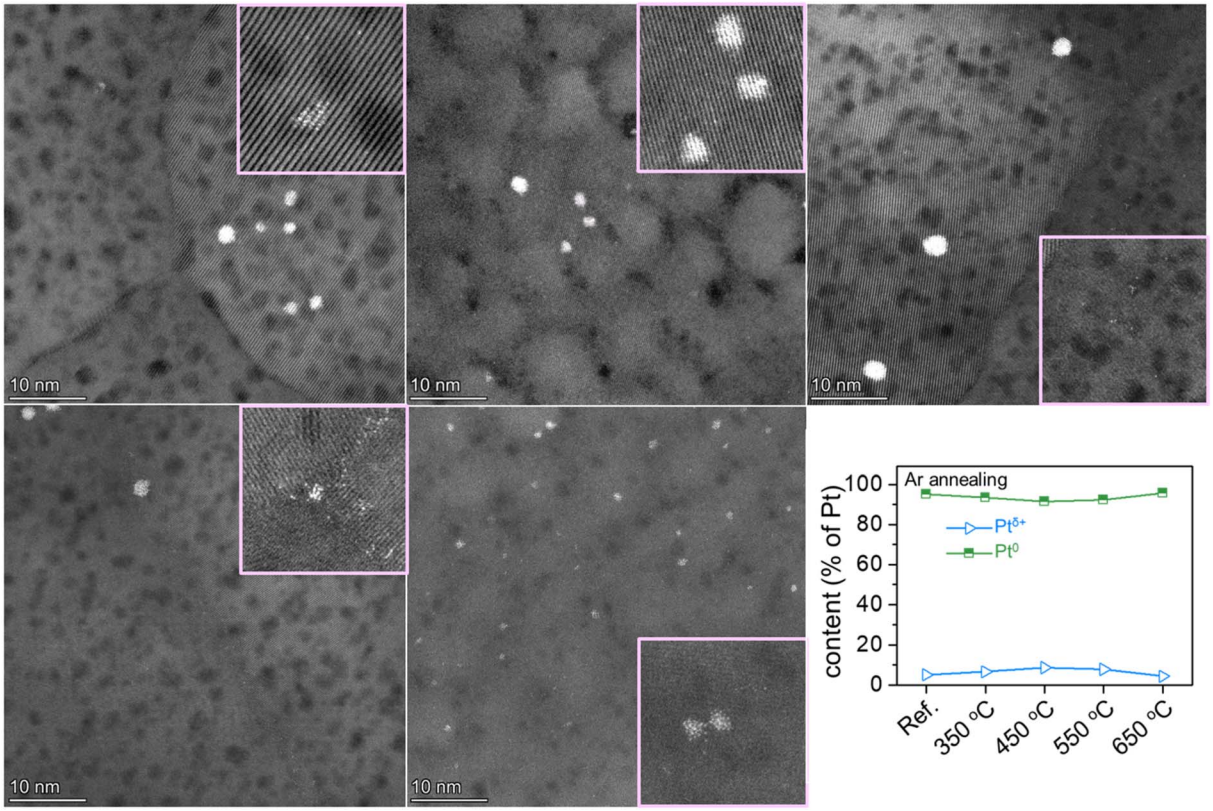

Fig. 7 Impact of thermal annealing in argon on the light-induced agglomeration behavior of Pt species on flat TiO_2 films (top left to bottom right: as-deposited; 350 °C, 1 h; 450 °C, 1 h; 550 °C, 1 h; 650 °C, 1 h; $Pt^{\delta+}$ to Pt^0 ratio as determined by XPS).

Table 2 Percentage of $Pt^{\delta+}$, density of SAs, rafts and NPs as well as the average NP size after different pre-annealing procedures and photocatalysis for 3 h (275 nm, 30 mW)

	As-deposited	350 °C, 1 h	450 °C, 1 h	550 °C, 1 h	650 °C, 1 h
$Pt^{\delta+}$ % (XPS)	5	6.6	8.6	7.7	4.3
#SA/μm^2	1×10^4	5×10^4	4×10^4	6×10^4	6×10^4
#Rafts/μm^2	2×10^3	5×10^3	3×10^3	8×10^3	2×10^4
#NPs/μm^2	1×10^3	4×10^3	1×10^3	2×10^3	8×10^3
d(NPs)/nm	1.8	2.4	2.9	3.1	1.8

activity.[58,72] As described above O_vs may play a key role in (i) stabilizing SAs in potentially the right coordination environment and (ii) acting as co-catalytic sites as recently reported for Pd[33] and Pt[30] on TiO_2 supports. Thus, whereas agglomeration in electro- and photocatalysis takes place close to room temperature due to H adsorption weakening the binding energy to the support and enhancing the self-diffusion of Pt by orders of magnitude,[73] thermal agglomeration requires elevated temperatures to overcome the Pt binding energy towards the TiO_2 substrate sites. In this context, elevated temperatures will lead to the generation of additional point defects such as O_vs on the support, which serve as additional anchoring sites for SAs partially stabilizing the system. Thermal annealing also helps to guide the SAs to the most stable anchoring sites on the substrates, since here the binding energy is the highest and consequently the Pt surface diffusion kinetics are the lowest.

Conclusion and outlook

In conclusion, our study demonstrates the feasibility of thermal treatments for fine-tuning the state of Pt as SAs, rafts, or 3D nanoparticles, and thus presents a tool for optimizing the Pt-speciation towards a maximum photocatalytic activity. We find that the photocatalytic activity of a Pt SA decorated sample annealed at 550 °C is more than five times higher as compared to that of the as-deposited one. *Ex situ* HRSTEM investigations reveal that the Pt dispersion and agglomeration state can be tuned by the treatment temperatures. While in any case a combination of SAs, rafts and NPs exists, overall, higher annealing temperatures lead to larger NPs (but still co-existing with SAs on the support). *In situ* investigations in the gas cell reveal details of the microscopic mechanism of agglomeration. At 250 °C, a high density of small 2D SA clusters (rafts) is formed

that then act either as nuclei and grow further or dissolve with increasing temperature. Since the structure of the mainly 2D object is far from that of the final NP, we also reveal a non-classical nucleation pathway meaning that the initial nuclei exhibit a different structure as compared to Pt NPs in equilibrium. The dissolution of initially formed nuclei documented *in situ* by high-resolution imaging demonstrates the detachment of Pt atoms and assemblies from ill-defined nuclei as well as from the NP on an atomic scale. Here, an increasing number of initially formed clusters dissolved with increasing temperature, while others grow further into stable and crystalline Pt NPs. In addition, the *in situ* as well as *ex situ* structural data documents the importance of predominant heterogeneous nucleation taking place at grain boundaries during thermally-induced agglomeration. Moreover, we demonstrate that thermal pre-annealing decisively influences later light-induced agglomeration during photocatalytic applications. Here, the non-annealed sample is most prone to agglomeration within minutes,[17] while annealed samples agglomerate, but to a much lower relative extent. Correlating the structural and electronic data after photocatalysis with the activity data indicates that SAs (in the right coordination environment and electronic state) are likely the most active sites during photocatalysis. The above consideration shows that – for a most effective use of Pt and a maximized activity and stability – on the one hand, strategies that shift the SA to agglomerate ratio towards the SA side are needed; on the other hand, the residual SAs can be trapped in a "right" structural environment (*e.g.* in the vicinity of O_Vs).

Methods

Formation of TiO_2 layers on Si/SiO_2 and SiN_x membranes

20 nm thick amorphous TiO_2 films were produced on the viewing windows of DENSsolutions climate chips as well as on Si/SiO_2 substrates by magnetron sputtering. The films were then crystallized *via in situ* heating in the climate system (700 mbar Ar atmosphere) for 30 min at 400 °C and within a conventional heating furnace for 1 h in an Ar atmosphere, respectively. Alternatively, the crystallization was achieved during the thermal studies with pre-loaded Pt SAs.

Deposition of Pt SAs on TiO_2 layers

The Pt SAs were produced on the crystalline TiO_2 layers *via* a facile reactive deposition method,[17,21,53] whereas the *ex situ* samples and chips were immersed in aqueous 2 mM and 0.05 mM H_2PtCl_6:$6H_2O$ solutions, respectively. All samples were kept in the dark for 1 h, while the backside was covered in order to only expose the TiO_2 functionalized side to the precursor solution. The membranes were subsequently washed with deionized water and dried in an N_2 atmosphere. In a separate experiment a lower Pt SA loading (0.005 mM H_2PtCl_6) on the amorphous TiO_2 layers was realized. The estimated Pt loading produced on the surface is equal to 0.14 at% (for 0.005 mM H_2PtCl_6), 0.47 at% (for 0.05 mM H_2PtCl_6), and 0.78 at% (for 2 mM H_2PtCl_6), respectively.[21]

Photocatalytic H_2 evolution

Photocatalytic H_2 evolution performance of the Pt SA-loaded TiO_2 anatase layers was evaluated under UV illumination. The samples were placed in a quartz reactor containing 50 vol% methanol (hole scavenger) aqueous solution (10 mL), which was subsequently purged with Ar for 15 min. After that, the reactor was sealed, and illumination with an LED ($\lambda = 275$ nm, power density of 20 mW cm^{-2}, exposure area = 1.2 cm × 1.2 cm) was carried out for a specified duration. A gas chromatograph (GCMS-QO2010SE, SHIMADZU) equipped with a thermal conductivity detector (TCD) was used to determine the amount of H_2 generated at specific time intervals.

SEM and XPS characterization

The surface and cross-section morphologies of the samples were investigated using a field-emission scanning electron microscope (FE-SEM, S-4800, Hitachi). The chemical composition of samples was analyzed by X-ray photoelectron spectroscopy (XPS, PHI 5600). All XPS spectra were shifted to a standard Ti 2p binding energy in anatase of 458.5 eV and the peak deconvolution was carried out by MultiPak software.

Ex situ STEM imaging

HAADF STEM imaging was conducted utilizing an aberration-corrected Thermo Fisher Scientific Spectra 200 operating at 200 keV. Images were taken at 960 kx as well as 1.8 Mx and various different positions each. For that a beam convergence angle of 15 mrad, a collection angle of 56–200 mrad, a beam current below 30 pA, and dwell times of 20 µs and 30 µs have been used.

In situ STEM imaging

High-resolution HAADF STEM imaging was performed at a double corrected FEI Titan Themis^3 300 operating at 300 kV. The beam convergence angle was 15.7 mrad. The collection angle was 38–200 mrad at a dwell time of 10 µs and 30–184 mrad at a dwell time of 2 µs for the 0.05 mM and 0.005 mM samples, respectively. To avoid drift due to charging of the membrane and to minimize the influence of the electron beam, the beam current was below the sensitivity limit of the screen of 30 pA. The DENSsolutions climate system was utilized for *in situ* heating and control of the atmosphere. In all *in situ* thermal studies, an Ar atmosphere with a pressure of 700 mbar and 0.3 mL min^{-1} flow rate was maintained.

Segmentation of STEM images

For statistical analysis of the particle size and density, STEM images were segmented using the software (Fiji is Just) ImageJ utilizing the Trainable Weka Segmentation plugin within a human-in-the-loop approach. The segmentation was trained with respect to three classes, namely, SAs, agglomerates and background/substrate. Typically, 20 to 30 areas per class were chosen as reference, while the segmentation result was stepwise checked. Further, the resulting segmentation was analyzed with the particle analyzer of Fiji. Here, edges were excluded whereas

all other segmented SA and NP areas were analyzed. Subsequently, the results were classified within three classes: (i) SAs, (ii) rafts, and (iii) NPs. For that a maximum size/diameter of 4 Å corresponding to the (100) lattice spacing of anatase and 1 nm have been chosen to classify SAs and rafts as displayed in Tables 1 and 2, respectively. Everything beyond 1 nm is classified as NP.

Data availability

Related files are available online upon publication at **https://doi.org/10.5281/zenodo.14507308**.

Author contributions

J. Will: conceptualization, data curation, formal analysis, investigation, methodology, validation, visualization, writing – original draft, writing – review & editing. N. Denisov: formal analysis, investigation, visualization, writing – original draft, writing – review & editing. S. Qin: data curation, formal analysis, investigation, visualization, writing – original draft, writing – review & editing. M. Wu: investigation. Y. Wang: investigation. H. Kim: investigation. N. Karpstein: investigation, writing – review & editing. M. Dierner: formal analysis, investigation, visualization. P. Schmuki: conceptualization, funding acquisition, methodology, resources, supervision, writing – original draft, writing – review & editing. E. Spiecker: conceptualization, funding acquisition, resources, supervision, validation, writing – review & editing.

Conflicts of interest

The authors declare no competing financial interest.

Acknowledgements

J. W., M. W. and E. S. acknowledge the Collaborative Research Centre SFB 1452—Catalysis at Liquid Interfaces (project 431791331). The authors would like to acknowledge DFG and the Operational Program Research, Development and Education (European Regional Development Fund, Project No. CZ.02.1.01/0.0/0.0/15_003/0000416 of the Ministry of Education, Youth and Sports of the Czech Republic) for financial support. Further, Ronald Spruit (DENSSolutions) is acknowledged for his assistance and guidance during the initial data acquisition in the climate system.

References

1 J. Xing, J. F. Chen, Y. H. Li, W. T. Yuan, Y. Zhou, L. R. Zheng, H. F. Wang, P. Hu, Y. Wang, H. J. Zhao, Y. Wang and H. G. Yang, Stable isolated metal atoms as active sites for photocatalytic hydrogen evolution, *Chemistry*, 2014, **20**(8), 2138–2144.

2 C. Gao, J. Low, R. Long, T. Kong, J. Zhu and Y. Xiong, Heterogeneous Single-Atom Photocatalysts: Fundamentals and Applications, *Chem. Rev.*, 2020, **120**(21), 12175–12216.

3 F. Zhang, Y. Zhu, Q. Lin, L. Zhang, X. Zhang and H. Wang, Noble-metal single-atoms in thermocatalysis, electrocatalysis, and photocatalysis, *Energy Environ. Sci.*, 2021, **14**(5), 2954–3009.

4 Z.-H. Xue, D. Luan, H. Zhang and X. W. Lou, Single-atom catalysts for photocatalytic energy conversion, *Joule*, 2022, **6**(1), 92–133.

5 S.-M. Wu and P. Schmuki, Single Atom Cocatalysts in Photocatalysis, *Adv. Mater.*, 2025, **37**, 2414889.

6 B. Wang, H. Cai and S. Shen, Single Metal Atom Photocatalysis, *Small Methods*, 2019, **3**(9), 1800447.

7 Y. Chen, S. Ji, C. Chen, Q. Peng, D. Wang and Y. Li, Single-Atom Catalysts: Synthetic Strategies and Electrochemical Applications, *Joule*, 2018, **2**(7), 1242–1264.

8 J. He, P. Liu, R. Ran, W. Wang, W. Zhou and Z. Shao, Single-atom catalysts for high-efficiency photocatalytic and photoelectrochemical water splitting: distinctive roles, unique fabrication methods and specific design strategies, *J. Mater. Chem. A*, 2022, **10**(13), 6835–6871.

9 Y. Zhao, Y. Guo, X. F. Lu, D. Luan, X. Gu and X. W. Lou, Exposing Single Ni Atoms in Hollow S/N-Doped Carbon Macroporous Fibers for Highly Efficient Electrochemical Oxygen Evolution, *Adv. Mater.*, 2022, **34**(35), 2203442.

10 B. Xia, Y. Zhang, J. Ran, M. Jaroniec and S. Z. Qiao, Single-Atom Photocatalysts for Emerging Reactions, *ACS Cent. Sci.*, 2021, **7**(1), 39–54.

11 S.-M. Wu, L. Wu, N. Denisov, Z. Badura, G. Zoppellaro, X.-Y. Yang and P. Schmuki, Pt Single Atoms on TiO2 Can Catalyze Water Oxidation in Photoelectrochemical Experiments, *J. Am. Chem. Soc.*, 2024, **146**(24), 16363–16368.

12 H. Jung, G. Cha, H. Kim, J. Will, X. Zhou, E. Spiecker, J. Breu and P. Schmuki, Ultrathin Ti-Deficient TiO2 Nanosheets with Pt Single Atoms Enable Efficient Photocatalytic Nitrate Reduction to Ammonia, *J. Am. Chem. Soc.*, 2025, **147**(11), 9049–9055.

13 C. f. Li, W. g. Pan, Z. r. Zhang, T. Wu and R. t. Guo, Recent Progress of Single-Atom Photocatalysts Applied in Energy Conversion and Environmental Protection, *Small*, 2023, **19**(22), 2300460.

14 Y. Shi, Z. R. Ma, Y. Y. Xiao, Y. C. Yin, W. M. Huang, Z. C. Huang, Y. Z. Zheng, F. Y. Mu, R. Huang, G. Y. Shi, Y. Y. Sun, X. H. Xia and W. Chen, Electronic metal-support interaction modulates single-atom platinum catalysis for hydrogen evolution reaction, *Nat. Commun.*, 2021, **12**(1), 3021.

15 P. Zhou, I. A. Navid, Y. Ma, Y. Xiao, P. Wang, Z. Ye, B. Zhou, K. Sun and Z. Mi, Solar-to-hydrogen efficiency of more than 9% in photocatalytic water splitting, *Nature*, 2023, **613**(7942), 66–70.

16 K. Rigby and J.-H. Kim, Deciphering the issue of single-atom catalyst stability, *Curr. Opin. Chem. Eng.*, 2023, **40**, 100921.

17 N. Denisov, S. Qin, J. Will, B. N. Vasiljevic, N. V. Skorodumova, I. A. Pasti, B. B. Sarma, B. Osuagwu, T. Yokosawa, J. Voss, J. Wirth, E. Spiecker and P. Schmuki, Light-Induced Agglomeration of Single-Atom Platinum in Photocatalysis, *Adv. Mater.*, 2023, **35**(5), e2206569.

18 X. Zhou, Y. Wang, N. Denisov, H. Kim, J. Kim, J. Will, E. Spiecker, A. Vaskevich and P. Schmuki, Pt Single Atoms Loaded on Thin-Layer TiO2 Electrodes: Electrochemical and Photocatalytic Features, *Small*, 2024, **20**, 2404064.
19 P. Tang, H. J. Lee, K. Hurlbutt, P. Y. Huang, S. Narayanan, C. Wang, D. Gianolio, R. Arrigo, J. Chen, J. H. Warner and M. Pasta, Elucidating the Formation and Structural Evolution of Platinum Single-Site Catalysts for the Hydrogen Evolution Reaction, *ACS Catal.*, 2022, **12**(5), 3173–3180.
20 S. Qin, N. Denisov, J. Will, J. Kolařík, E. Spiecker and P. Schmuki, A Few Pt Single Atoms Are Responsible for the Overall Co-Catalytic Activity in Pt/TiO2 Photocatalytic H2 Generation, *Sol. RRL*, 2022, **6**(6), 2101026.
21 S. Qin, J. Will, H. Kim, N. Denisov, S. Carl, E. Spiecker and P. Schmuki, Single Atoms in Photocatalysis: Low Loading Is Good Enough, *ACS Energy Lett.*, 2023, **8**(2), 1209–1214.
22 D. Wang, Z.-P. Liu and W.-M. Yang, Revealing the Size Effect of Platinum Cocatalyst for Photocatalytic Hydrogen Evolution on TiO2 Support: A DFT Study, *ACS Catal.*, 2018, **8**(8), 7270–7278.
23 L. Liu, D. M. Meira, R. Arenal, P. Concepcion, A. V. Puga and A. Corma, Determination of the Evolution of Heterogeneous Single Metal Atoms and Nanoclusters under Reaction Conditions: Which Are the Working Catalytic Sites?, *ACS Catal.*, 2019, **9**(12), 10626–10639.
24 Y. Wang, N. Denisov, S. Qin, D. S. Goncalves, H. Kim, B. B. Sarma and P. Schmuki, Stable and Highly Active Single Atom Configurations for Photocatalytic H(2) Generation, *Adv. Mater.*, 2024, **36**(25), e2400626.
25 Y.-H. Li, Z.-S. Huang, M.-Y. Qi and Z.-R. Tang, Benchmark comparison study on metal single atom versus metal nanoparticle in photoredox catalysis: Which is better?, *Mol. Catal.*, 2024, **567**, 114474.
26 Y. H. Li, J. Xing, X. H. Yang and H. G. Yang, Cluster Size Effects of Platinum Oxide as Active Sites in Hydrogen Evolution Reactions, *Chem. - Eur. J.*, 2014, **20**(39), 12377–12380.
27 C. Wang, K. Wang, Y. Feng, C. Li, X. Zhou, L. Gan, Y. Feng, H. Zhou, B. Zhang, X. Qu, H. Li, J. Li, A. Li, Y. Sun, S. Zhang, G. Yang, Y. Guo, S. Yang, T. Zhou, F. Dong, K. Zheng, L. Wang, J. Huang, Z. Zhang and X. Han, Co and Pt Dual-Single-Atoms with Oxygen-Coordinated Co–O–Pt Dimer Sites for Ultrahigh Photocatalytic Hydrogen Evolution Efficiency, *Adv. Mater.*, 2021, **33**(13), 2003327.
28 S. Zhang, M. Hou, Y. Zhai, H. Liu, D. Zhai, Y. Zhu, L. Ma, B. Wei and J. Huang, Dual-Active-Sites Single-Atom Catalysts for Advanced Applications, *Small*, 2023, **19**(42), 2302739.
29 A. Zhu, Y. Cao, N. Zhao, Y. Jin, Y. Li, L. Yang, C. Zhang, Y. Gao, Z. Zhang, Y. Zhang and W. Xie, Geminal Synergy in Pt-Co Dual-Atom Catalysts: From Synthesis to Photocatalytic Hydrogen Production, *J. Am. Chem. Soc.*, 2024, **146**(48), 33002–33011.
30 J. Zhang, P. Qiao, H. Tan, L. Cui, Z. Zhou, D. Lin, Y. Tuo and Y. Qin, Species Heterogeneity and Synergy to Boost Photocatalytic Hydrogen Evolution, *ACS Catal.*, 2024, **14**(20), 15699–15712.
31 J. Zhang, Y. Pan, D. Feng, L. Cui, S. Zhao, J. Hu, S. Wang and Y. Qin, Mechanistic Insight into the Synergy between Platinum Single Atom and Cluster Dual Active Sites Boosting Photocatalytic Hydrogen Evolution, *Adv. Mater.*, 2023, **35**(25), 2300902.
32 X. Zhang, M. Zhang, Y. Deng, M. Xu, L. Artiglia, W. Wen, R. Gao, B. Chen, S. Yao, X. Zhang, M. Peng, J. Yan, A. Li, Z. Jiang, X. Gao, S. Cao, C. Yang, A. J. Kropf, J. Shi, J. Xie, M. Bi, J. A. van Bokhoven, Y.-W. Li, X. Wen, M. Flytzani-Stephanopoulos, C. Shi, W. Zhou and D. Ma, A stable low-temperature H2-production catalyst by crowding Pt on α-MoC, *Nature*, 2021, **589**(7842), 396–401.
33 T. Wang, X. Tao, X. Li, K. Zhang, S. Liu and B. Li, Synergistic Pd Single Atoms, Clusters, and Oxygen Vacancies on TiO2 for Photocatalytic Hydrogen Evolution Coupled with Selective Organic Oxidation, *Small*, 2021, **17**(2), 2006255.
34 H. V. Thang, G. Pacchioni, L. DeRita and P. Christopher, Nature of stable single atom Pt catalysts dispersed on anatase TiO2, *J. Catal.*, 2018, **367**, 104–114.
35 L. Chen, R. R. Unocic, A. S. Hoffman, J. Hong, A. H. Braga, Z. Bao, S. R. Bare and J. Szanyi, Unlocking the Catalytic Potential of TiO(2)-Supported Pt Single Atoms for the Reverse Water-Gas Shift Reaction by Altering Their Chemical Environment, *JACS Au*, 2021, **1**(7), 977–986.
36 L. DeRita, S. Dai, K. Lopez-Zepeda, N. Pham, G. W. Graham, X. Pan and P. Christopher, Catalyst Architecture for Stable Single Atom Dispersion Enables Site-Specific Spectroscopic and Reactivity Measurements of CO Adsorbed to Pt Atoms, Oxidized Pt Clusters, and Metallic Pt Clusters on TiO2, *J. Am. Chem. Soc.*, 2017, **139**(40), 14150–14165.
37 A. Corma, P. Serna, P. Concepción and J. J. Calvino, Transforming Nonselective into Chemoselective Metal Catalysts for the Hydrogenation of Substituted Nitroaromatics, *J. Am. Chem. Soc.*, 2008, **130**(27), 8748–8753.
38 T. J. Lee and Y. G. Kim, Redispersion of supported platinum catalysts, *J. Catal.*, 1984, **90**(2), 279–291.
39 X. Zhang, Z. Li, W. Pei, G. Li, W. Liu, P. Du, Z. Wang, Z. Qin, H. Qi, X. Liu, S. Zhou, J. Zhao, B. Yang and W. Shen, Crystal-Phase-Mediated Restructuring of Pt on TiO2 with Tunable Reactivity: Redispersion versus Reshaping, *ACS Catal.*, 2022, **12**(6), 3634–3643.
40 J. Cai, A. Cao, Z. Wang, S. Lu, Z. Jiang, X.-Y. Dong, X. Li and S.-Q. Zang, Surface oxygen vacancies promoted Pt redispersion to single-atoms for enhanced photocatalytic hydrogen evolution, *J. Mater. Chem. A*, 2021, **9**(24), 13890–13897.
41 Y. Wang, S. Qin, N. Denisov, H. Kim, Z. Bad'ura, B. B. Sarma and P. Schmuki, Reactive Deposition Versus Strong Electrostatic Adsorption (SEA): A Key to Highly Active Single Atom Co-Catalysts in Photocatalytic H(2) Generation, *Adv. Mater.*, 2023, e2211814.
42 Y. Wang, S. Lee, J. Zhou, J. Fu, A. Foucher, E. Stach, L. Ma, N. Marinkovic, S. Ehrlich, W. Zheng and D. G. Vlachos, Higher loadings of Pt single atoms and clusters over

reducible metal oxides: application to C–O bond activation, *Catal. Sci. Technol.*, 2022, **12**(9), 2920–2928.

43 F. Pesty, H.-P. Steinrück and T. E. Madey, Thermal stability of Pt films on TiO2(110): evidence for encapsulation, *Surf. Sci.*, 1995, **339**(1), 83–95.

44 T. N. Geppert, M. Bosund, M. Putkonen, B. M. Stühmeier, A. T. Pasanen, P. Heikkilä, H. A. Gasteiger and H. A. El-Sayed, HOR Activity of Pt-TiO2-Y at Unconventionally High Potentials Explained: The Influence of SMSI on the Electrochemical Behavior of Pt, *J. Electrochem. Soc.*, 2020, **167**(8), 084517.

45 E. M. Larsson, J. Millet, S. Gustafsson, M. Skoglundh, V. P. Zhdanov and C. Langhammer, Real Time Indirect Nanoplasmonic in Situ Spectroscopy of Catalyst Nanoparticle Sintering, *ACS Catal.*, 2012, **2**(2), 238–245.

46 V. P. Zhdanov, E. M. Larsson and C. Langhammer, Novel aspects of Ostwald ripening of supported metal nanoparticles, *Chem. Phys. Lett.*, 2012, **533**, 65–69.

47 S. B. Simonsen, I. Chorkendorff, S. Dahl, M. Skoglundh, J. Sehested and S. Helveg, Ostwald ripening in a Pt/SiO2 model catalyst studied by in situ TEM, *J. Catal.*, 2011, **281**(1), 147–155.

48 S. B. Simonsen, I. Chorkendorff, S. Dahl, M. Skoglundh, J. Sehested and S. Helveg, Direct Observations of Oxygen-induced Platinum Nanoparticle Ripening Studied by In Situ TEM, *J. Am. Chem. Soc.*, 2010, **132**, 7968.

49 M. Farnesi Camellone, F. Dvořák, M. Vorokhta, A. Tovt, I. Khalakhan, V. Johánek, T. Skála, I. Matolínová, S. Fabris and J. Mysliveček, Adatom and Nanoparticle Dynamics on Single-Atom Catalyst Substrates, *ACS Catal.*, 2022, **12**(9), 4859–4871.

50 G. Cha, A. Mazare, I. Hwang, N. Denisov, J. Will, T. Yokosawa, Z. Badura, G. Zoppellaro, A. B. Tesler, E. Spiecker and P. Schmuki, A facile "dark"-deposition approach for Pt single-atom trapping on facetted anatase TiO2 nanoflakes and use in photocatalytic H2 generation, *Electrochim. Acta*, 2022, **412**, 140129.

51 W. Liu, J.-g. Wang, W. Li, X. Guo, L. Lu, X. Lu, X. Feng, C. Liu and Z. Yang, A shortcut for evaluating activities of TiO2 facets: water dissociative chemisorption on TiO2-B (100) and (001), *Phys. Chem. Chem. Phys.*, 2010, **12**(31), 8721–8727.

52 S. J. Pennycook and D. E. Jesson, High-resolution Z-contrast imaging of crystals, *Ultramicroscopy*, 1991, **37**(1), 14–38.

53 S. Hejazi, S. Mohajernia, B. Osuagwu, G. Zoppellaro, P. Andryskova, O. Tomanec, S. Kment, R. Zboril and P. Schmuki, On the Controlled Loading of Single Platinum Atoms as a Co-Catalyst on TiO(2) Anatase for Optimized Photocatalytic H(2) Generation, *Adv. Mater.*, 2020, **32**(16), e1908505.

54 P. Petzoldt, M. Eder, S. Mackewicz, M. Blum, T. Kratky, S. Günther, M. Tschurl, U. Heiz and B. A. J. Lechner, Tuning Strong Metal–Support Interaction Kinetics on Pt-Loaded TiO2(110) by Choosing the Pressure: A Combined Ultrahigh Vacuum/Near-Ambient Pressure XPS Study, *J. Phys. Chem. C*, 2022, **126**(38), 16127–16139.

55 B.-J. Hsieh, M.-C. Tsai, C.-J. Pan, W.-N. Su, J. Rick, H.-L. Chou, J.-F. Lee and B.-J. Hwang, Tuning metal support interactions enhances the activity and durability of TiO2-supported Pt nanocatalysts, *Electrochim. Acta*, 2017, **224**, 452–459.

56 B. Fritsch, M. Wu, A. Hutzler, D. Zhou, R. Spruit, L. Vogl, J. Will, H. Hugo Pérez Garza, M. März, M. P. M. Jank and E. Spiecker, Sub-Kelvin thermometry for evaluating the local temperature stability within in situ TEM gas cells, *Ultramicroscopy*, 2022, **235**, 113494.

57 C. Dessal, A. Sangnier, C. Chizallet, C. Dujardin, F. Morfin, J. L. Rousset, M. Aouine, M. Bugnet, P. Afanasiev and L. Piccolo, Atmosphere-dependent stability and mobility of catalytic Pt single atoms and clusters on gamma-Al(2)O(3), *Nanoscale*, 2019, **11**(14), 6897–6904.

58 L. DeRita, J. Resasco, S. Dai, A. Boubnov, H. V. Thang, A. S. Hoffman, I. Ro, G. W. Graham, S. R. Bare, G. Pacchioni, X. Pan and P. Christopher, Structural evolution of atomically dispersed Pt catalysts dictates reactivity, *Nat. Mater.*, 2019, **18**(7), 746–751.

59 Y. Zhou, C. L. Muhich, B. T. Neltner, A. W. Weimer and C. B. Musgrave, Growth of Pt Particles on the Anatase TiO2 (101) Surface, *J. Phys. Chem. C*, 2012, **116**(22), 12114–12123.

60 J. Lee, J. Yang, S. G. Kwon and T. Hyeon, Nonclassical nucleation and growth of inorganic nanoparticles, *Nat. Rev. Mater.*, 2016, **1**(8), 1–16.

61 P. Schweizer, A. Sharma, L. Pethö, E. Huszar, L. M. Vogl, J. Michler and X. Maeder, Atomic scale volume and grain boundary diffusion elucidated by in situ STEM, *Nat. Commun.*, 2023, **14**(1), 7601.

62 S. Wei, A. Li, J. C. Liu, Z. Li, W. Chen, Y. Gong, Q. Zhang, W. C. Cheong, Y. Wang, L. Zheng, H. Xiao, C. Chen, D. Wang, Q. Peng, L. Gu, X. Han, J. Li and Y. Li, Direct observation of noble metal nanoparticles transforming to thermally stable single atoms, *Nat. Nanotechnol.*, 2018, **13**(9), 856–861.

63 M. Moliner, J. E. Gabay, C. E. Kliewer, R. T. Carr, J. Guzman, G. L. Casty, P. Serna and A. Corma, Reversible Transformation of Pt Nanoparticles into Single Atoms inside High-Silica Chabazite Zeolite, *J. Am. Chem. Soc.*, 2016, **138**(48), 15743–15750.

64 H. Meltzman, D. Chatain, D. Avizemer, T. M. Besmann and W. D. Kaplan, The equilibrium crystal shape of nickel, *Acta Mater.*, 2011, **59**(9), 3473–3483.

65 T. H. Zhang and X. Y. Liu, Nucleation: what happens at the initial stage?, *Angew Chem. Int. Ed. Engl.*, 2009, **48**(7), 1308–1312.

66 T. W. van Deelen, C. Hernández Mejía and K. P. de Jong, Control of metal-support interactions in heterogeneous catalysts to enhance activity and selectivity, *Nat. Catal.*, 2019, **2**(11), 955–970.

67 S. Duan, R. Wang and J. Liu, Stability investigation of a high number density Pt(1)/Fe(2)O(3) single-atom catalyst under different gas environments by HAADF-STEM, *Nanotechnology*, 2018, **29**(20), 204002.

68 L. Piccolo, Restructuring effects of the chemical environment in metal nanocatalysis and single-atom catalysis, *Catal. Today*, 2021, **373**, 80–97.

69 J. Will, E. Wierzbicka, M. Wu, K. Götz, T. Yokosawa, N. Liu, A. B. Tesler, M. Stiller, T. Unruh, M. Altomare, P. Schmuki and E. Spiecker, Hydrogenated anatase TiO2 single crystals: defects formation and structural changes as microscopic origin of co-catalyst free photocatalytic H2 evolution activity, *J. Mater. Chem. A*, 2021, **9**(44), 24932–24942.

70 S. Ji, Y. Chen, X. Wang, Z. Zhang, D. Wang and Y. Li, Chemical Synthesis of Single Atomic Site Catalysts, *Chem. Rev.*, 2020, **120**(21), 11900–11955.

71 S. Mohajernia, P. Andryskova, G. Zoppellaro, S. Hejazi, S. Kment, R. Zboril, J. Schmidt and P. Schmuki, Influence of Ti3+ defect-type on heterogeneous photocatalytic H2 evolution activity of TiO2, *J. Mater. Chem. A*, 2020, **8**(3), 1432–1442.

72 W. Zang, J. Lee, P. Tieu, X. Yan, G. W. Graham, I. C. Tran, P. Wang, P. Christopher and X. Pan, Distribution of Pt single atom coordination environments on anatase TiO(2) supports controls reactivity, *Nat. Commun.*, 2024, **15**(1), 998.

73 S. Horch, H. T. Lorensen, S. Helveg, E. Lægsgaard, I. Stensgaard, K. W. Jacobsen, J. K. Nørskov and F. Besenbacher, Enhancement of surface self-diffusion of platinum atoms by adsorbed hydrogen, *Nature*, 1999, **398**(6723), 134–136.